Journal of Theoretical and Computational Chemistry
Vol. 18, No. 6 (2019) 1950029 (25 pages)

DOI: 10.1142/S0219633619500299

World Scientific
www.worldscientific.com

Spectral and quantum chemical analysis of ethyl 4-[3-(adamantan-1-yl)-4-phenyl-5-sulfanylidene-4,5-dihydro-1H-1,2,4-triazole-1-yl]methylpiperazine-1-carboxylate

Hanan A. Al-Ghulikah

Department of Chemistry, College of Sciences
Princess Nourah Bint Abdulrahman University
Riyadh 11671, Saudi Arabia

Darya Meniailava and Ulada Vysotskaya

Faculty of Physics, Belarusian State University
4 Nezaležnaści Ave., Minsk 220030, Belarus

Anna Matsukovich

B. I. Stepanov Institute of Physics
National Academy of Science of Belarus
68 Nezaležnaści Ave., Minsk 220072, Belarus

Ali A. El-Emam

Department of Medicinal Chemistry
Faculty of Pharmacy, University of Mansoura
Mansour 35516, Egypt

Maksim Shundalau*

Faculty of Physics, Belarusian State University
4 Nezaležnaści Ave., Minsk 220030, Belarus

A. N. Sevchenko Institute of Applied Physical
Problems at Belarusian State University
7 Kurčataŭ Str., Minsk 220108, Belarus
shundalov@bsu.by

Received 27 June 2019
Accepted 19 September 2019
Published 23 October 2019

The Fourier transform infrared and Raman spectra of the adamantane-based compound ethyl 4-[3-(adamantan-1-yl)-4-phenyl-5-sulfanylidene-4,5-dihydro-1H-1,2,4-triazol-1-yl]methylpiperazine-1-carboxylate were recorded in the ranges of 3200–650 cm^{-1} and 3200–150 cm^{-1}, respectively. The UV/Vis spectrum of solution of the title compound in ethanol was measured in the range of 450–200 nm. The DFT calculations at the B3LYP/cc-pVDZ and B3LYP/cc-pVTZ

*Corresponding author.

levels of the theory were performed to obtain the equilibrium geometric structure and to predict vibrational IR and Raman spectra of the title molecule. The TDDFT calculations at the CAM-B3LYP/cc-pVTZ level of the theory, as well as MRPT calculations at the CASSCF(4,5)/XMCQDPT2 level of the theory were carried out to reproduce the electronic absorption spectrum. The experimental IR, Raman and UV/Vis spectra were interpreted on the basis of results of quantum chemical modeling. Based on Mulliken and Löwdin atomic population analysis, it was established that the compound under study exhibits features of an intramolecular charge transfer.

Keywords: Adamantane-based compounds; FTIR spectrum; Raman spectrum; UV/Vis spectrum; density functional theory; multi-reference perturbation theory.

1. Introduction

Adamantane derivatives have found wide practical applications in the field of medicine as possible candidates for the drug design and drugs delivery.[1,2] The pronounced lipophilicity, chemical and thermal stability, conformational rigidity of adamantyl cage are reflected on the adamantane-based derivatives leading to improvement of their pharmacokinetic properties.[3] After the development of amantadine as an efficient antiviral drug against influenza A viruses,[4] and as anti-parkinsonian drug,[5] numerous adamantane derivatives were developed and currently used as effective therapeutic agents. The major pharmacological activities displayed by adamantane-based derivatives are the antiviral,[6–10] anticancer,[11–13] antibacterial and antifungal,[14–17] antimalarial,[18] anti-inflammatory,[19,20] and hypoglycemic activities.[21] On the other hand, 1,2,4-triazole derivatives were reported to exhibit diverse biological activities including antifungal,[22] anti-inflammatory[23] and anti-cancer activities.[24]

In continuation of our ongoing interest in the pharmacological and structural properties of adamantane derivatives,[25–28] on the basis of experimental (infrared (IR), Raman and Ultraviolet (UV)/Vis spectroscopy) and theoretical (Density Functional Theory (DFT), Time-Dependent Density Functional Theory (TDDFT) and Multi-Reference Perturbation Theory (MRPT) calculations) methods, we report herein the geometric, electronic and spectral characteristics of the title adamantane-triazole hybrid derivative.

The main goal of the study is to use the results of the quantum chemical calculations to investigate the spectral properties and to perform a complete and noncontradictory interpretation of the spectra obtained for achieving a better understanding of the physicochemical properties of adamantane-based compounds as promising candidates for the design of new drugs.

2. Experimental Details

2.1. *Instruments*

The IR spectrum of the title compound for the crystalline phase was measured using an FT-IR spectrometer Nexus (Thermo Nicolet, USA) supplied with an IR

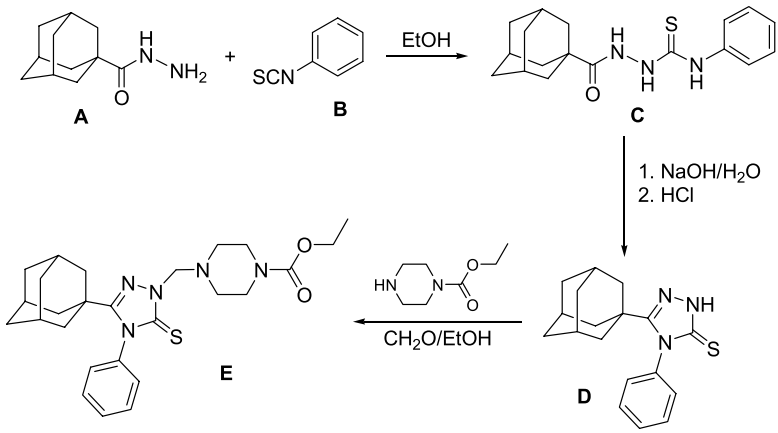

Fig. 1. The synthetic approach of the title compound (**E**).

microscope setup Continuum (Thermo Fisher Scientific, USA) with a 15×-objective. Measurements in the range of 3200–650 cm^{-1} were performed in the reflection mode, where the probe radiation entered small area of thinned crystalline powder on the top of a reflective surface.

The Raman scattering spectrum also for the crystalline phase was measured in the range of 3200–150 cm^{-1} using a compact solid-state cw-Nd:YAG laser (second harmonic, 532 nm wavelength), a holographic notch filter, a grating spectrometer (600 grooves per mm) Spectra Pro500i (Acton Research, USA) and a silicon cooled CCD-camera.

The electronic absorption (UV/Vis) spectrum of the ethanol solution of the title compound was measured by a Cary 500 (Varian) spectrophotometer in the range of 450–200 nm. Since the main absorption bands lie in the near UV range, care has been taken to minimize contribution from the solvent. For this reason, a cell with the solvent was used in the reference channel during measurements to ensure correct subtraction of solvent contribution.

2.2. *Chemical synthesis of the title compound*

The title compound (**E**) was synthesized starting with adamantane-1-carbohydrazide (**A**) via reaction with phenyl isothiocyanate (**B**) to yield the intermediate thiosemicarbazide derivative (**C**), which was cyclized to the triazole derivative (**D**). The reaction of (**D**) with ethyl piperazine-1-carboxylate and formaldehyde solution, in ethanol, at room temperature yielded the title compound (**E**) in 80% yield (Fig. 1).[17] The structure of the title compound was established by ^{1}H and ^{13}C NMR and single crystal X-ray crystallography.[29]

3. Computational Details

The calculations of the structural and vibrational spectral characteristics of the title compound were realized with the use of the quantum chemical package

GAMESS-US.[30,31] The optimization of the equilibrium structure, calculations of the Hessians (force fields), normal coordinates analysis and intensities for the IR and Raman spectra were performed using the standard Dunning's cc-pVDZ and cc-pVTZ basis sets[32] by DFT methods with the help of the hybrid B3LYP functional.[33–35] The modern DFT methods are a high-reliable tool to establish the molecular structure of the ground state of organic compounds.[36] In its turn a high accuracy of the structural predictions is a prerequisite for the adequate spectra simulation.

Firstly, the full geometric optimization without any constraints was carried out. The vibrational frequencies were calculated in the harmonic approximation. For this, Hessians (matrices of second derivatives of the energy with respect of nuclear coordinates, or force constants matrices) were derived by seminumerical method. This method does analytical first derivatives and numerical second ones. The diagonalization of Hessian gives squares of the vibrational frequencies. In the force field computation, we took into account two displacements (one positive and one negative) in each Cartesian direction. This gives a small improvement ($\sim$20–50 cm^{-1}, or $\sim$1%) in the accuracy of the computations of vibrational frequencies and this avoids the appearance of imaginary frequencies for low-frequency deformation modes in some cases. Since the calculated values at the B3LYP/cc-pVTZ level of theory harmonic frequencies of the high-frequency stretching modes usually exceed the experimental ones by 3–4%, such improvement in accuracy is very significant. Analysis of the calculated Hessian matrices testifies the absence of imaginary frequencies, confirming the stability of the equilibrium structure. The intensities of IR bands and Raman lines were calculated assuming their proportionality to squares of derivatives of the electric dipole moment and polarizabilities with respect to normal coordinates, respectively.[36]

TDDFT is currently widely used for electronic spectra simulation of polyatomic molecular systems.[37] It is known that quantum chemical calculations using, for example, the hybrid functional B3LYP in terms of the TDDFT approximation display deviations of the excited state energies from the available experimental values up to 0.4 eV.[38] Especially this is typical for molecular systems with charge transfer. The presence of phenyl, piperazine and triazole groups in the structure of the title molecule allows one to classify it as a molecular system that may exhibit the intramolecular charge transfer (ICT). In this case, the Coulomb-attenuating method (CAM)[39] makes it possible to qualitatively and quantitatively improve the results of the calculations.

The calculations of spectral and energetic characteristics of the excited singlet electronic states for the title compound were performed in terms of the TDDFT approximation using the cc-pVTZ basis set[32] and the hybrid CAM-B3LYP functional.[39] The calculations were carried out also by the GAMESS-US quantum chemical package. The influence of solvent (ethanol) was taken into account in the approximation of the Solvation Model Density (SMD).[40]

An alternative to the TDDFT method is multi-reference approximation (for example, MRPT). Recently,[26–29] we have shown that the *ab initio* calculations at the

multi-reference CASSCF/XMCQDPT2 (Complete Active Space Self-Consistent Field/eXtended Multi-Configuration Quasi-Degenerate 2nd Order Perturbation Theory)[41] level of theory successfully explain the UV/Vis absorption spectra of the N′-(adamantan-2-ylidene)benzohydrazide,[26] 3-(adamantan-1-yl)-4-ethyl-1-[(4-phenylpiperazin-1-yl)methyl]-1H-1,2,4-triazole-5(4H)-thione,[27] 3-(adamantan-1-yl)-1-[(4-benzylpiperazin-1-yl)methyl]-4-phenyl-1H-1,2,4-triazole-5(4H)-thione,[27] and 3-(adamantan-1-yl)-4-phenyl-1-[(4-phenylpiperazin-1-yl)methyl]-1H-1,2,4-triazole-5(4H)-thione[28] molecules.

The CASSCF/XMCQDPT2 calculations for the title molecule were performed using the Firefly[42] quantum chemical package with the standard cc-pVTZ basis set. Firstly, the CASSCF calculations with the state-averaged (SA) procedure were done. The active space for the CASSCF calculations comprises four electrons and five orbitals. The SA-CASSCF(4,5) procedure was realized for three singlet and two triplet states. Finally, the calculations for singlets were performed at the XMCQDPT2 (Ref. 41) level of theory. All 127 lowest double occupied orbitals are included in the perturbation-based calculation. The ISA shift of 0.001 was used in the present approach.

The knowledge of the structure of the compound under investigation allows one to predict the so-called indices of its biological activities/inactivities (Pa/Pi), which mean the probabilities of the presence (Pa) or absence (Pi) of a biological activity of a particular species. Biological activity is a property of a chemical compound that characterizes its interaction with biological systems and exhibits any therapeutic, cosmetic or other properties.[43] The calculation of biological activity indices was carried out using the PASS database (prediction of activity spectra for substances).[44] PASS-online[45] makes it possible to predict more than 4000 kinds of biological activity on the basis of the structure of the compound. The main idea[46] is that similar structures have similar biological activities or in other words the molecular structure determines the spectrum of biological activities.

4. Results and Discussion

4.1. *Geometric structure*

The title compound, namely ethyl 4-[3-(adamantan-1-yl)-4-phenyl-5-sulfanylidene-4,5-dihydro-1H-1,2,4-triazol-1-yl]methylpiperazine-1-carboxylate ($C_{26}H_{35}N_5O_2S$), the equilibrium structure of which is shown in Fig. 2, represents a structure consisting of conformationally stable fragments of phenyl, triazole and piperazine rings, as well as methylene, ethyl, carbonyl, and adamantyl groups connected by single bonds. Moreover, piperazine, triazole and methylene groups form the molecular skeleton, to which all other groups are attached. Due to steric effects rotation around single bonds is unavailable that leads to rigid structure of the compound indicating the absence of structural conformers. The only exception is related to the rotation around the single bond between oxygen atom and carbon atom of ethyl group that raises two possible

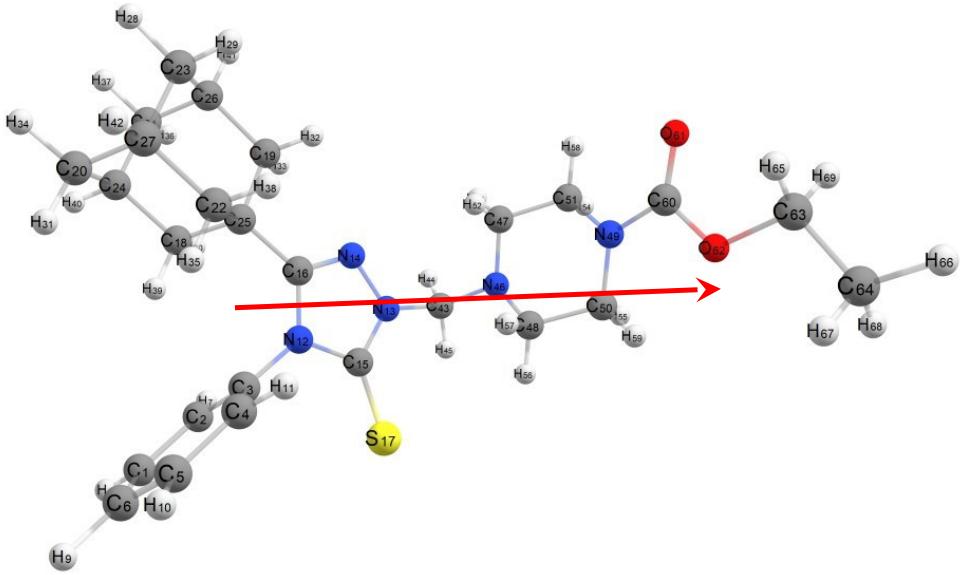

Fig. 2. The optimized structure of the title compound obtained at the B3LYP/cc-pVTZ level of theory. Arrow shows the direction of dipole moment of the molecule and labels and digits show the numbering of atoms.

orientation of ethyl group. But these two conformers possess almost the same energy (the difference is less than 10 cm^{-1}).

The experimental values of the geometric parameters (values of bond lengths, bond angles and dihedral angles) obtained by X-ray analysis for the crystalline phase of the title compound.[29] We should note that most of the structural parameters were determined experimentally,[29] with the exception of C–H bond lengths. Moreover, the values of the selected parameters seem to be incorrect. The C–H bond lengths of the adamantyl and phenyl fragments were found to be 0.99–1.0 Å and 0.95 Å, respectively. However, it is known that the experimental value for adamantyl fragment is 1.112 Å (Ref. 47) and for phenyl −1.09 Å.[48] The same situation is observed for CH bonds in piperazine ring, methylene and ethyl fragments. Based on this, we can conclude that the lengths chosen as parameters do not correspond to the actual values and the discussion of the comparison of the calculated data with the values of these parameters will not be given, since it leads to large errors (up to 9–14%).

The results of calculations of geometry parameters performed in the B3LYP/cc-pVDZ and B3LYP/cc-pVTZ approximations for the gas phase of the title compound are in agreement with the experimental data obtained for the crystalline phase. The calculated geometric parameters are presented and compared with the experimental data in Table S1 (see Supplementary Information). For most bond lengths, the deviations of the calculated values from the experimental values do not exceed 1%. The exceptions are the bond lengths comprising nitrogen (C–N and N–N of the piperazine and triazole rings and C–N bonds between methylene and piperazine and

methylene and triazole fragments) and oxygen (for the single bond between the oxygen atom and the carbon atom of the ethyl fragment), as well as for the C–C bond in the ethyl fragment. For the mentioned bond lengths, the deviations were 1.1–1.8% (C–N), 1.1% (N–N), 1.1–1.5% (C–O) and 2.4–2.7% (C–C).

Such errors are supposed to be connected with the presence of heteroatoms in structure and have already occurred earlier and been discussed.[25,27,28] Planar angles follow the same pattern: deviations of calculated angles from experimental ones are not more than 1%. For planar angles, which include nitrogen and oxygen atoms, an error not exceeding 4.6% is observed. However, the largest (7.7%) value of the deviation was for the angle between the carbon atom in methylene fragment and the N–C bond in piperazine ring. The errors mentioned may be related to the choice of the basis set and the functional used for calculations, as well as to the fact that calculations were performed for gas phase in contrast to experiment, which was performed for solid samples. In general, according to the comparative table, the values of the geometric parameters obtained using doubly and triply splitted basis sets differ little. Meanwhile, using a larger basis leads to some decrease in the average error for bond lengths (the average error is 0.49% for cc-pVTZ and 0.72% for cc-pVDZ) and a slight decrease for bond angles (0.68% for cc-pVTZ and 0.70% for cc-pVDZ). Therefore, for optimization of the geometry for the compound under study, in order to reduce the time spent on computational process, one can use cc-pVDZ basis. In our case, optimization procedure is followed by calculations of vibrational frequencies, for which the expansion of basis set can reduce the error associated with overestimation of the frequencies, for example, for stretching vibrations.

4.2. *Vibrational spectra*

For the compound under consideration, IR and Raman spectra were predicted at the B3LYP/cc-pVTZ level of theory in harmonic approximation. As it was mentioned, the structure of the studied compound includes various functional groups, and in most cases the vibrations are localized on one of those functional groups. Such functional groups as adamantyl, phenyl, or ethyl have characteristic frequencies and vibrational modes, and therefore the assignment of the corresponding bands in the spectra does not cause any particular difficulties. However, other groups, such as piperazine and triazole, form the molecular skeleton and the vibrations localized on these groups often interact with each other, which makes the spectra interpretation difficult. Based on the calculations, we carried out a complete interpretation of IR and Raman vibrational spectra for the title compound, which has 201 vibrational modes.

Figure 3 shows the experimental and calculated IR and Raman spectra of the studied compound. The results of the interpretation of the experimentally obtained IR and Raman spectra on the basis of the calculated ones are given in Table 1, where the normal modes are denoted as follows: ν denotes stretching; δ denotes bending; ρ denotes rocking; σ denotes scissoring; ω denotes wagging; γ denotes twisting;

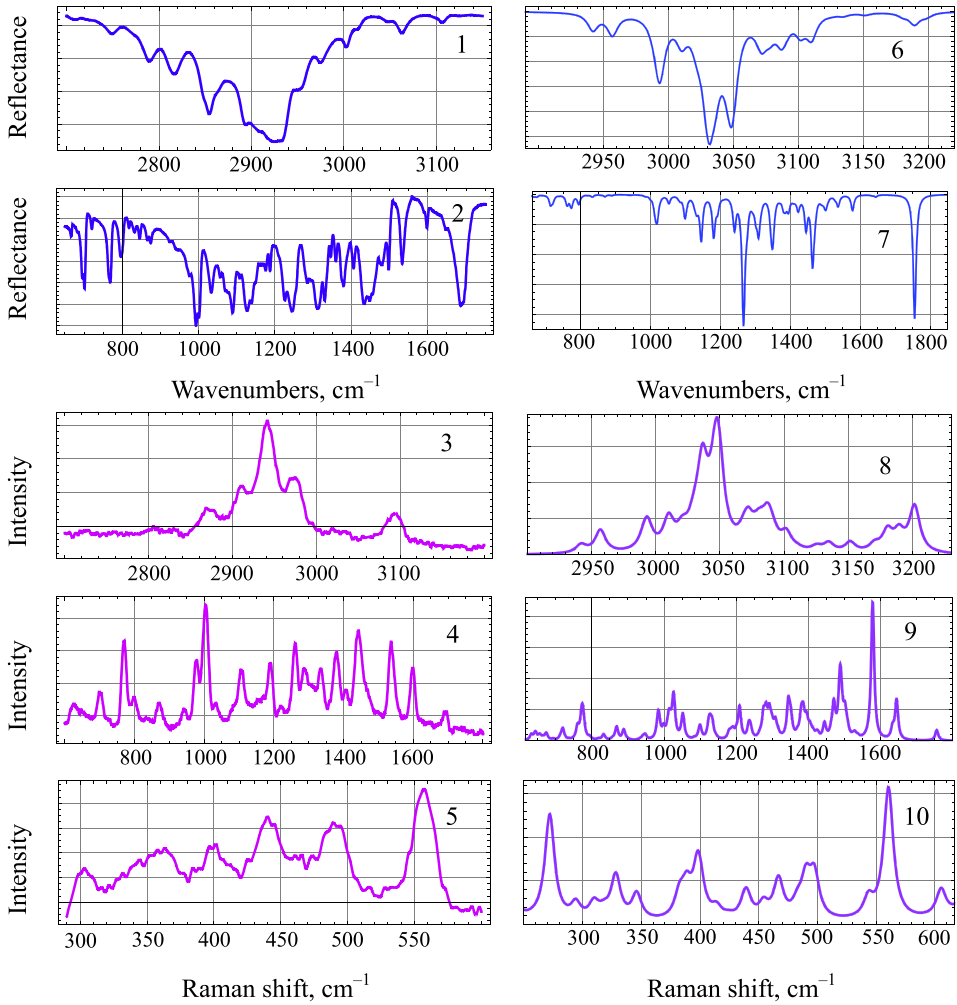

Fig. 3. Experimental (1–5) and calculated (B3LYP/cc-pVTZ) (6–10) IR (1, 2, 6, 7) and Raman spectra (3–5, 8–10) of the title compound.

i.p. denotes in-plane bending; o.o.p. denotes out-of-plane bending vibrations. Band and line intensities I_{IR} and I_{Raman} are normalized to the strongest band or line; vs. denotes very strong; s denotes strong; m denotes medium; w denotes weak; vw denotes very weak; sh denotes shoulder. The following symbols were also used to designate functional groups: Ph denotes phenyl group, M denotes methylene group, P denotes piperazine, A denotes adamantyl fragment, T denotes triazole fragment, Et denotes ethyl group.

The calculated frequencies as usual for harmonic approximation exceeded the experimental values for C–H stretching vibrations by 3.1–5.5% (in the region about 2940–3200 cm^{-1}) and reproduced very well (overestimation is 0.2–2.8%) the

Table 1. Assignment of vibrational frequencies of the title compound.

Experimental		Calculated			
ν_{IR}, cm^{-1}	ν_{Raman}, cm^{-1}	ν, cm^{-1}	I_{IR}	I_{Raman}	Assignment
	3095 w	3202	0.00	0.70	νCH(Ph)
	3089 w	3198	0.01	0.01	νCH(Ph)
	3086 w	3189	0.05	0.27	νCH(Ph)
	3080 m	3180	0.00	0.31	νCH(Ph)
3062 w	3061 vw	3170	0.00	0.11	νCH(Ph)
3049 w	3046 vw	3151	0.01	0.15	νCH(P)
	3034 w	3135	0.01	0.13	νCH(P)
	3025 w	3125	0.00	0.08	νCH_2(M)
3018 sh	3019 w	3110	0.09	0.03	νCH3 + νCH_2(Et)
3003 w	3004 w	3102	0.07	0.25	νCH3(Et)
	2984 sh				2×1496
		3091	0.02	0.16	νCH(P)
2976 m	2975 m	3087	0.09	0.43	νCH_2(A)
		3084	0.01	0.04	νCH_2(A)
	2969 m	3081	0.01	0.23	νCH_2 + νCH3(Et)
2949 m	2942 vs	3078	0.05	0.11	νCH_2(A)
2931 sh		3072	0.10	0.38	νCH_2(P) + νCH_2(M)
		3068	0.01	0.12	νCH_2(M) + νCH_2(P)
		3050	0.05	0.25	νCH_2(Et)
2926 vs		3049	0.22	0.51	νCH_2(A)
		3047	0.11	1.00	νCH_2(A) + νCH(A)
		3044	0.01	0.14	νCH_2(A) + νCH(A)
		3044	0.04	0.09	νCH_2(A)
	2911 m	3037	0.04	0.64	νCH_3(Et)
2912 s		3036	0.12	0.53	νCH + νCH_2(A)
2908 sh		3032	0.27	0.10	νCH + νCH_2(A)
	2901 sh	3029	0.14	0.22	νCH + νCH_2(A)
2895 s		3022	0.07	0.07	νCH + νCH_2(A)
	2876 w	3020	0.00	0.18	νCH + νCH_2(A)
2865 sh	2868 w	3011	0.03	0.11	νCH + νCH_2(A)
2854 s		3010	0.03	0.15	νCH + νCH_2(A)
		3010	0.03	0.19	νCH + νCH_2(A)
2848 w		2993	0.24	0.43	νCH(P)
		2991	0.03	0.08	νCH(P)
	2830 w	2957	0.08	0.35	νCH(P)
		2942	0.07	0.12	νCH(P)
2818 w	2821 vw				1456 + 1360
	2805 w				1443 + 1362
2791 w					1479 + 1313
2773 sh					1406 + 1360
	2758 w				1537 + 1221
2750 vw	2752 vw				1456 + 1296; 1406 + 1346
1686 vs	1690 w	1755	0.99	0.02	νC = O
1647 w	1650 w				1001 + 646; 993 + 654; 1090 + 557
1599 w	1598 s	1644	0.02	0.07	νCC(Ph) + δ(i.p.)CCC(Ph)
		1633	0.01	0.02	νCC(Ph) + δ(i.p.)CCC(Ph)
1533 m	1537 vs	1578	0.12	0.24	νCN(T)
1498 m	1496 vw	1536	0.09	0.00	νCC(Ph) + δ(i.p.)CCC(Ph)
		1528	0.02	0.01	σCH_2(Et) + δCH_3(Et)
		1523	0.00	0.00	σCH_2(A)

Table 1. (*Continued*)

Experimental		Calculated			
ν_{IR}, cm^{-1}	ν_{Raman}, cm^{-1}	ν, cm^{-1}	I_{IR}	I_{Raman}	Assignment
		1508	0.01	0.01	$\sigma CH_2(P) + \sigma CH_2(M)$
1479 m	1477 sh	1501	0.03	0.01	$\sigma CH_2(A) + \sigma CH_2(P)$
		1501	0.03	0.01	$\sigma CH_2(A) + \sigma CH_2(P) + \sigma CH_2(M)$
		1501	0.01	0.00	$\sigma CH_2(A)$
		1501	0.01	0.03	$\sigma CH_2(Et) + \delta CH_3(Et)$
		1498	0.03	0.00	$\sigma CH_2(A)$
		1493	0.02	0.01	$\sigma CH_2(P)$
		1490	0.00	0.02	$\nu CC(Ph) + \sigma CH_2(P)$
1456 s		1490	0.01	0.01	$\nu CC(Ph) + \sigma CH_2(P)$
		1488	0.00	0.03	$\sigma CH_2(A)$
		1488	0.01	0.03	$\delta CH_3(Et)$
		1486	0.00	0.04	$\sigma CH_2(A)$
	1443 s	1470	0.09	0.06	$\sigma CH_2(M)$
1448 s		1463	0.54	0.01	$\nu CN(P) + \gamma CH_2(P) + \omega CH_2(Et)$
1433 vs		1444	0.25	0.03	$\nu CN(T) + \gamma CH_2(M)$
	1407 w	1425	0.01	0.01	$\sigma CH_2(M) + \omega CH_2(P)$
1406 m		1422	0.10	0.00	$\delta CH_3(Et) + \omega CH_2(Et)$
		1413	0.01	0.01	$\omega CH_2(P) + \gamma CH_2(M) + \omega CH_3(Et)$
		1408	0.02	0.01	$\gamma CH_2(M) + \omega CH_2(P) + \omega CH_3(Et)$
1381 s	1379 s	1404	0.00	0.01	$\omega CH_2(A)$
		1402	0.00	0.00	$\omega CH_2(A)$
		1398	0.00	0.00	$\omega CH_2(A)$
1375 sh		1395	0.08	0.02	$\omega CH_2(P) + \omega CH_2(M)$
		1392	0.03	0.00	$\omega CH_2(Et) + \omega CH_3(Et)$
1360 m	1362 sh	1385	0.07	0.04	$\omega CH_2(A) + \nu CN(T) + \gamma CH_2(M)$
		1381	0.00	0.00	$\omega CH_2(A)$
1346 m	1344 sh	1380	0.07	0.04	$\nu CN(T) + \omega CH_2(A) + \gamma CH_2(M) + \gamma CH_2(P)$
		1369	0.01	0.01	$\omega CH_2(P)$
		1360	0.00	0.00	$\omega CH_2(A)$
		1356	0.00	0.00	$\nu CC(Ph)$
		1354	0.00	0.00	$\omega CH_2(A)$
1313 s		1348	0.23	0.01	$\gamma CH_2(M) + \nu CN(T) + \nu CN(P)$
		1344	0.14	0.06	$\nu CN(T) + \nu CS(T) + \gamma CH_2(M) + \delta CCH(A) + \delta NCH(P)$
1296 m	1294 m	1325	0.00	0.00	$\nu CC(Ph) + \delta CCH(Ph)$
		1317	0.00	0.00	$\nu CC(A) + \gamma CH_2(A)$
		1315	0.05	0.01	$\delta CCC(A) + \delta CCH(A) + \delta NCN(T)$
		1313	0.00	0.00	$\nu CC(A) + \delta CCH(A)$
1284 m	1286 m	1308	0.27	0.03	$\nu CN(T) + \nu CC(A)$
		1301	0.12	0.01	$\nu CN(P) + \delta HCN(P) + \gamma CH_2(M)$
		1297	0.01	0.01	$\gamma CH_2(Et) + \delta CH_3(Et)$
1259 sh	1260 s	1292	0.04	0.04	$\delta CH_2(A) + \delta CNC(T)$
		1283	0.00	0.04	$\delta CCH(A)$
		1275	0.15	0.04	$\delta CNC(T) + \delta CCH(A)$
1246 vs	1245 sh	1265	1.00	0.01	$\nu C–O + \gamma CH_2(P)$
1225 s	1220 vw	1240	0.24	0.02	$\nu CN(P) + \gamma CH_2(P) + \gamma CH_2(M) + \nu CS(T)$
1211 sh		1235	0.01	0.02	$\gamma CH_2(P)$
1188 m	1190 s	1209	0.01	0.03	$\gamma CH_2(A)$
		1209	0.00	0.03	$\gamma CH_2(A)$
		1200	0.00	0.01	δ(i.p.)CCH(Ph)

Table 1. (*Continued*)

Experimental		Calculated			
ν_{IR}, cm^{-1}	ν_{Raman}, cm^{-1}	ν, cm^{-1}	I_{IR}	I_{Raman}	Assignment
1176 m	1170 vw	1191	0.10	0.01	νCN(P) + νCN(T) + γCH_2(P)
		1186	0.00	0.01	δ(i.p.)CCH(Ph)
		1183	0.01	0.00	ρCH_2(Et) + ρCH_3(Et)
1153 sh	1152 vw	1180	0.31	0.01	νC(M)N(P) + δNCH(P)
1136 s	1138 vw	1144	0.35	0.00	νCO + δNCH(P)
		1143	0.00	0.00	γCH_2(A)
		1134	0.00	0.00	γCH_2(A)
		1134	0.01	0.02	νCC(Et) + δCCH(Et) + δCC(Et)O
		1131	0.08	0.01	νCN(P) + νCN(T) + γCH_2(M) + ρCH_2(A)
1109 m	1107 m	1128	0.03	0.02	ρCH_2(A)
		1125	0.02	0.01	ρCH_2(A)
		1123	0.00	0.01	ρCH_2(A)
		1104	0.01	0.00	νCC(Ph) + δ(i.p.)CCH(Ph)
		1100	0.02	0.02	δCCC(A) + δCCC(Ph)+ δCNC(T) + ρCH_2(P)
1090 vs	1086 sh	1098	0.15	0.01	νCC(P) + ρCH_2(P)
1057 m	1057 vw	1084	0.03	0.00	νCN(T) + νCN(P) + ρCH_2(M)
		1079	0.01	0.00	ρCH_2(P) + δCCN(P)
	1032 w	1053	0.01	0.01	νCC(Ph) + δ(i.p.)CCC(Ph)
1034 s		1052	0.05	0.03	νCO + νCC(Et) + δCCN(P)
		1050	0.00	0.00	νCC(A)
		1049	0.00	0.00	νCC(A)
		1044	0.00	0.00	νCC(A)
		1026	0.01	0.07	νCC(Ph) + δ(i.p.)CCC(Ph)
1001 sh	1003 vs	1018	0.16	0.01	νCN(P) + ρCH_2(P)
993 vs		1014	0.09	0.03	δ(i.p.)CCC(Ph) + νCN(P)
		1012	0.02	0.01	δ(o.o.p.)CCH(Ph)
		1010	0.03	0.01	νNN(T) + νCC(P) + ρCH_2(M)
976 m	979 s	999	0.02	0.02	νCC(Et) + νCC(P) + νO–C(Et)
		992	0.00	0.00	δ(o.o.p.)CCH(Ph)
947 w	943 w	986	0.00	0.02	νCC(A)
		984	0.00	0.02	νCC(A)
		983	0.00	0.02	νCC(A)
926 w	923 w	948	0.00	0.01	νCC(A) + δ(o.o.p.)CCH(Ph)
		942	0.00	0.00	νCC(A) + δ(o.o.p.)CCH(Ph)
		942	0.00	0.00	νCC(A) + δ(o.o.p.)CCH(Ph)
		935	0.00	0.00	νCN(P) + ρCH_2(M)
894 vw	897 vw	900	0.00	0.00	ρCH_2(A)
		899	0.00	0.00	ρCH_2(A)
		897	0.00	0.00	ρCH_2(A)
876 w	875 w	888	0.01	0.02	νCO + νCC(Et) + δCCH(Et)
866 w	865 sh	869	0.02	0.02	νCC(A)
847 w	843 vw	857	0.00	0.00	δCCN(P) + ρCH_2(P)
		857	0.00	0.00	δ(o.o.p.)CCH(Ph)
831 w	833 vw	833	0.02	0.01	νCO + δCCH(Et) + νCN(P)
818 w	818 vw	820	0.00	0.00	νCC(A) + δCCC(A)
		819	0.00	0.00	νCC(A) + δCCC(A)
		815	0.00	0.00	γCH_2(Et) + δ(o.o.p.)CH_3(Et)
796 m	798 m	794	0.07	0.00	δ(o.o.p.)CCH(Ph) + δ(o.o.p.)CCC(Ph)
		777	0.00	0.02	δCNC(P) + δ(o.o.p.)N(P)C = O

Table 1. (*Continued*)

Experimental		Calculated			
ν_{IR}, cm^{-1}	ν_{Raman}, cm^{-1}	ν, cm^{-1}	I_{IR}	I_{Raman}	Assignment
		774	0.04	0.03	δ(o.o.p.)CCH(Ph) + δCCC(A)
	771 s	771	0.06	0.03	δCNC(P) + δ(o.o.p.)N(P)C = O
768 s		760	0.08	0.02	δCCC(A) + δN(P)C(M)N(T)
721 w	724 w	737	0.00	0.00	ωNCN(T)
702 s	704 m	720	0.05	0.02	δ(o.o.p.)CCC(Ph)
696 sh	699 sh	713	0.07	0.00	δ(o.o.p.)CCC(Ph)
		693	0.00	0.00	δCCC(A) + δCNC(T) + δ(i.p.)CCC(Ph)
683 sh	679 vw	674	0.02	0.01	δ(o.o.p)CNC(T) + ρCH$_2$(P)
667 w	666 vw	665	0.01	0.00	δCCN(P) + δN(P)C–O
		657	0.00	0.00	δCCC(A)
	654 vw	655	0.00	0.01	δCCC(A)
	646 vw	644	0.04	0.01	δ(o.o.p.)CCH(Ph) + δCCN(P) + δNCN(T)
	626 w	633	0.00	0.01	δ(i.p.)CCC(Ph)
	599 vw	605	0.03	0.00	σCNC(P) + δN(T)C(M)N(P)
	558 w	560	0.01	0.02	νC(T)S + δNCN(T) + ρCH$_2$(M)
	545 sh	543	0.02	0.00	δN(P)C–O + δCCH(Et) + δCCN(P)
	494 w	497	0.00	0.01	δCCN(P) + δ(o.o.p.)CCC(Ph) + δCH$_2$(M)
	489 sh	490	0.00	0.00	δCCN(P)
	482 sh	483	0.01	0.00	δ(o.o.p.)CCC(Ph) + δCCC(A) + δCNC(P)
	466 vw	467	0.00	0.00	δCCC(A)
	446 w	454	0.01	0.00	δCCC(A) + δCNC(P)
	441 sh	440	0.00	0.00	δCCC(A)
		438	0.00	0.00	δCCC(A)
	425 vw	424	0.00	0.00	δ(o.o.p.)CCC(Ph)
	412 vw	415	0.00	0.00	δCCC(A)
		414	0.00	0.00	δCCC(A) + δCH$_2$(M)
	402 vw	400	0.00	0.00	δCH$_2$(M) + δCNC(P) + δCCC(A)
	397 sh	398	0.00	0.01	δCNC(P) + δCH$_2$(M)
	389 sh	388	0.00	0.00	δCCC(A) + δ(o.o.p.)CNN(T) + δCH$_2$(M)
	384 vw	382	0.04	0.00	δO–CC(Et) + δCNC(P) + δCH$_2$(M)
	363 w	346	0.00	0.00	δCCC(A) + δCNC(P) + δO–CC(Et)
	327 vw	328	0.01	0.01	δCCC(A) + δCNC(P) + δO–CC(Et)+ δCCC(Ph)
	317 vw	318	0.01	0.00	δCNC(P) + δC–O–C(Et) + δCCC(A)
	312 vw	314	0.00	0.00	δCCC(A)
	303 w	309	0.00	0.00	δCCC(A) + δCNN(T)
	298 sh	294	0.02	0.00	δ(o.o.p.)CNC(P)
	270 sh	272	0.00	0.01	δ(o.o.p.)CCC(Ph) + ρCH$_2$(P)
		259	0.00	0.00	ρCH3(Et) + ρCH$_2$(Et)
		238	0.00	0.00	δCCC(Ph) + ρCH$_2$(P)
		229	0.01	0.00	ρCH$_2$(P) + ρC–O–C(Et)
		210	0.00	0.01	δCCC(A) + δN(P)C(M)N(T)
		201	0.01	0.00	δCCC(A) + δN(P)C(M)N(T)
		173	0.01	0.00	δNC(T)S + δC(M)NC(P) + δC–O–C(Et)
		162	0.00	0.00	δ(o.o.p.)NC(T)S + δCNC(T)
		146	0.00	0.00	ωC–O–C(Et) + ρN(T)C(M)N(P)+ γNCN(T)
		121	0.00	0.00	ωC–O–C(Et) + ρCH$_2$(Et)
		115	0.00	0.01	σC(T)CC(A) + δCC(Ph)N(P) + δCC(Et)–O
		111	0.00	0.00	γO–C = O + γCNC(P)

Table 1. (*Continued*)

Experimental		Calculated			
ν_{IR}, cm^{-1}	ν_{Raman}, cm^{-1}	ν, cm^{-1}	I_{IR}	I_{Raman}	Assignment
		89	0.00	0.00	γC–O–C(Et) + δO–CC(Et)
		85	0.00	0.00	δCC(Ph)N(T) + δNC(T)C(A)+ γCN(P)C(M)
		66	0.00	0.00	δCC(Ph)N(T) + δNC(T)C(A) + δCN(P)–C
		60	0.00	0.01	δCC(Ph)N(T) + δNC(T)C(A)
		57	0.00	0.00	δO–CC(Et) + γC–O–C(Et) + δCNC(P)
		50	0.00	0.02	δCC(Ph)N(T) + δO–CC(Et)
		33	0.00	0.00	δO–CC(Et) + γCN(P)–C+ γCNC(P) + γO = C–O
		30	0.00	0.00	δCC(Ph)N(T) + δO–CC(Et)
		26	0.00	0.00	δCC(A)C(T) + δO–CC(Et)
		14	0.00	0.00	δCN(P)–C + δCC(Ph)N(T)
		9	0.00	0.00	δCN(P)–C + δC(T)CC(A)

frequencies in the middle IR region (660–1700 cm^{-1}). The Lorentzian profiles were used for broadening in calculated spectra. For consistency with experimental spectra, the values of full width at half maximum (FWHM) were taken 10 cm^{-1} for both IR and Raman spectra.

4.2.1. *Adamantyl fragment vibrations*

Adamantane is a tricyclic saturated hydrocarbon $C_{10}H_{16}$, the structure of which consists of six CH_2 and three CH bonds,[47,49] forming a "chair" conformation. The spectral regions of the adamantyl group include stretching vibrations of the CH and CC bonds, as well as scissoring, wagging, twisting, and rocking deformation vibrations of the CH and CH_2 bonds and skeletal vibrations of the CCC bonds.[47,49,50] It is known that the adamantane molecule possesses a high symmetry (T_d) and the vibrational frequencies in such case are not difficult to interpret. As a result of the monosubstitution of the adamantyl fragment the decrease of symmetry occurs and, therefore, a splitting of the observed vibration frequencies happens. It was previously established[50] that the stretching CH and CH_2 vibrations in the case of monosubstitution are located in the 2996–2945 cm^{-1} and 2952–2850 cm^{-1} regions, respectively.[49,50] Based on the calculated results, we assigned the bands 2976, 2949, 2926, 2912, 2895, 2865, and 2854 cm^{-1} in the IR spectrum and the peaks 2975, 2942, 2901, 2876, and 2868 cm^{-1} in the Raman spectrum as stretching CH and CH_2 vibrations of the adamantyl fragment. According to Ref. 50, scissoring vibrations of CH_2 can be found in the 1475–1440 cm^{-1} region. We also found the scissoring vibrations very close to this region: the bands 1479 cm^{-1} and 1456 cm^{-1} and line 1477 cm^{-1} in IR and Raman spectra, respectively. Due to the diminishing of the symmetry as a result of monosubstitution the wagging vibrations CH2 near 1350 cm^{-1} split and raise a particular sequence of bands in the range of 1400–1300 cm^{-1}.[49] Thus the bands 1381, 1360, 1346, and 1331 cm^{-1} and lines 1379, 1362,

1344, and 1335 cm^{-1} were assigned as corresponding to wagging vibrational modes. The twisting and rocking deformation vibrations of CH_2 can be found near 1200 cm^{-1} and 1100 cm^{-1} (Ref. 50) and in our case they appear in spectra as bands (lines) 1296 (1294), 1259 (1260), 1188 (1190), and 1136 (1138) cm^{-1} for twisting vibrations and 1109 (1107) cm^{-1} for rocking vibrations. Stretching vibrations of the CC bond of the adamantyl fragment lie near 800 cm^{-1}, and deformation vibrations of the adamantyl frame CCC can be found in the regions 780–740 cm^{-1} and 460–330 cm^{-1}.[49] This knowledge allows us to assign bands 866 cm^{-1} and 818 cm^{-1} and lines 865 cm^{-1} and 818 cm^{-1} to stretching vibrations of the CC, and bands 768, 696, 667 and peaks 699, 666, 466, 446, 441, 412, 389, 363, and 312 cm^{-1} to deformation vibrations of the adamantyl frame CCC.

4.2.2. *Phenyl group vibrations*

The vibrational frequencies of the phenyl ring correspond to the stretching vibrations of the CH and CC bonds, as well as to planar and out-of-plane vibrations of the CCC and CCH bonds.[51] For aromatic compounds, the stretching CH vibrations are located in the region of 3100–3000 cm^{-1}.[51] The vibrations of frame, as well as CC stretching vibrations are related to the absorption in the 1600–1585 cm^{-1} and 1500–1400 cm^{-1} region. It is also known that the bands of in-plane bending modes are located in the range of 1300–1000 cm^{-1}. The out-of-plane CH vibrations are observed in low-frequency range of 900–675 cm^{-1}. Taking into account the usual regions of vibrations of aromatic compounds,[51] we assigned bands 1599, 1498, 1456 cm^{-1} of IR spectrum and lines 1598 cm^{-1} and 1496 cm^{-1} of Raman spectrum to the stretching vibrations CC. The bands 1188, 1176 and 1034 cm^{-1} and lines 1190 cm^{-1} and 1170 cm^{-1} were identified as in-plane bending vibrations. The out-of-plane bending vibrations were found for 976, 926, 847, 796, 702, and 696 cm^{-1} bands and 979, 923, 843, 798, 704, 699, and 646 cm^{-1} lines of studied spectra.

4.2.3. *C = O and C–O vibrations*

It is known that ketones, carboxylic acids, aldehydes, carboxylic esters, and other compounds comprising C = O possess strong absorption band associated with the stretching vibration of C = O in the 1870–1540 cm^{-1} region.[51] The conjugation of C = O group with other groups causes the reduction of the observed frequency region. Thus, we identified strong band 1686 cm^{-1} in IR spectrum and line 1690 cm^{-1} in Raman spectrum as stretching C = O vibration. The stretching C–O vibrations for esters are located in the 1300–1000 cm^{-1} frequency range and the bands usually possess high intensity.[51] These stretching vibrations of C–O were found in spectra of the title compound as the bands 1246, 1136 and 1034 cm^{-1} and lines 1245 cm^{-1} and 1138 cm^{-1}.

4.2.4. *Ethyl and methylene vibrations*

Asymmetric and symmetric stretching vibrations of the CH_2 and CH_3 bonds of the ethyl group are observed in the regions 2950–3050 cm^{-1} and 2900–2995 cm^{-1},

respectively.[51] The methylene group CH_2 is located between two bulky rings and demonstrates a mixture of its normal modes with the triazole and piperazine ones. The IR spectrum band at 2931 cm^{-1} and the Raman spectrum line at 3025 cm^{-1} are defined as stretching CH_2 vibrations of methylene group. The stretching CH_3 vibrational bands and lines of ethyl group were assigned to 3018 cm^{-1} and 3003 cm^{-1} and 3019, 3004 cm^{-1}, respectively. We defined the lines 2969 cm^{-1} and 2911 cm^{-1} as being related to stretching CH_2 vibrations of ethyl group. Bending vibrations CH_3 are localized near 1375 cm^{-1} and 1450 cm^{-1}. And it is known for the former band to be overlapped with the bending vibrations (scissoring) of CH_2 group[51] which usually occur near 1465 cm^{-1}. The rocking vibrations of methylene group are observed near 720 cm^{-1}, wagging and twisting vibrations of CH_2 appear in the range of 1350–1150 cm^{-1}.[51] The bands (lines) 1456, 1406 (1407) and 1375 cm^{-1} in our spectra correspond to bending CH_3 vibrations, as well as the bands (lines) 1346 (1344), 1313 and 1284 (1286) cm^{-1} correspond to twisting CH_2 vibrations and 1176 (1170) cm^{-1} and 818 (818) cm^{-1} correspond to rocking CH_2 vibrations. Also, we have to note that it is difficult to identify these bending vibrations as they are mixed with the bending modes of other groups (triazole and piperazine ones).

4.2.5. *Piperazine ring vibrations*

The spectral region of the piperazine ring includes stretching vibrations of the CH, CC and CN bonds as well as deformation CH_2 modes. The stretching vibrations of CH bonds in heterocyclic structures occupy a region of 2800–3100 cm^{-1}.[52,53] Previously, it was found that piperazine stretching CH_2 vibrations occur at approximately 3087, 2987, 2914, 2853, and 2750 cm^{-1} for the IR spectrum[53] and at 2833 cm^{-1}, 2771 cm^{-1} for the Raman spectrum[53] and 2944 cm^{-1} for the IR spectrum.[52] However, the frequencies 2750 cm^{-1} and 2771 cm^{-1} are quite low for stretching modes of CH_2 and by their nature are very similar to overtones or combinations frequencies. Therefore, for this assignment, we slightly raised the lower limit for the frequency range of the mentioned stretching modes. Considering the above-mentioned, we assigned the bands 3049, 2976, 2931, and 2848 cm^{-1} in IR spectrum and the lines 3046, 2975, and 2830 cm^{-1} in Raman spectrum to stretching CH and CH_2 vibrations. The bending CH_2 modes (scissoring, wagging and rocking) for pure piperazine were found in the region of 1458–1431 cm^{-1},[52] near 1426 cm^{-1},[53] 1382 cm^{-1} (Ref. 52); 1390, 1364 and 1360 cm^{-1},[53] and near 852 cm^{-1},[52] respectively. For 1-phenylpiperazine,[54] scissoring modes appeared near 1407 cm^{-1} and wagging modes appeared near 1190 cm^{-1}. The bands 1346, 1331, 1211, and 1188 cm^{-1} in IR spectrum and lines 1407, 1344, 1335, and 1190 cm^{-1} in Raman spectrum were assigned as bending CH_2 vibrations. It has been established[51] that as a result of the interaction of heteroaromatic rings, it is not possible to distinguish individual vibration frequencies of the CC, CN and NN bonds. The stretching vibrations of heteroaromatic compounds appear in the same region (1600–1300 cm^{-1} (Ref. 51)) as vibrations of aromatic compounds, which complicates the interpretation and leads to the overlapping of vibrational bands.

In Ref. 47, the bands at 1177, 1115 and 933 cm^{-1} and the lines at 1184, 1109 and 836 cm^{-1} in IR and Raman spectra of the pure piperazine were assigned to the frame vibrations. According to Ref. 52, stretching CN vibrations occur at 1323, 1268, 1218, 1173, and 1055 cm^{-1} in IR and at 1294, 1120 and 1049 cm^{-1} in Raman spectrum. The CC stretching modes were observed at 1199 cm^{-1} (IR) and at 1186 cm^{-1} (Raman).[53] The bands in the studied IR spectrum 1225, 1176 and 1001 cm^{-1} and the lines 1220, 1170 and 1003 cm^{-1} in the Raman spectrum were assigned to the stretching CN and CC frame vibrations. The in-plane and out-of-plane bending modes of piperazine fragment are observed below 847 cm^{-1}.

4.2.6. *Triazole ring vibrations*

The triazole ring substituted by sulfur mainly exhibits stretching vibrations of CN, C = N, NN and CS bonds, deformations of the ring itself, as well as planar and out-of-plane vibrations of NH and CS bonds.[55,56] The stretching skeleton vibrations of triazole fragment (in our case CN, NN and CS) also interact with each other like the ones in the piperazine ring. Another difficulty is related to the fact that the frequencies of these stretching vibrations depend on the type of substitution. The bands and lines corresponding to breathing modes of the 1H-1,2,4-triazole ring previously were assigned at 1540,[55] 1495–1482,[55,56] 1473,[55] 1390–1361,[55,56] 1272–1255,[56] 1146,[56] 1190,[55] and 1062–1055 cm^{-1}.[56] The bands and lines 1533 (IR), 1537 (Raman), 1346 (IR), 1344 (Raman), 1284 (IR), 1286 (Raman), 1259 (IR), and 1260 (Raman) cm^{-1} were assigned as stretching triazole ring modes. Bending modes of triazole ring are observed below 768 cm^{-1} (see Table 1).

The bands at 1313, 1225, 1176, 1153, 1057, and 993 cm^{-1} in the IR spectrum and lines at 1220, 1170, 1152, and 1057 cm^{-1} in the Raman spectrum are associated with the stretching delocalized modes, where the delocalization occurs on the molecular skeleton and different functional groups comprising the molecule.

4.3. *UV/Vis spectrum*

The experimental UV/Vis absorption spectrum of the title compound in ethanol solution as well as calculated ones are shown in Fig. 4. The maximum of the long-wavelength band in the experimental spectrum (Fig. 4, curve 1) corresponds to the wavelength of 256 nm and the shortwave band is located around 200 nm. It is not possible to establish the exact value of shortwave band, since in this wavelength region ethanol absorption begins and there is also a restriction on wavelengths associated with the operating range of the UV/Vis spectrometer.

The simulated UV/Vis spectra were obtained in the terms of the CAM-B3LYP/cc-pVTZ, CAM-B3LYP/cc-pVTZ + SMD (ethanol) and CASSCF(4,5)/XMCQDPT2 approximations. The results of the calculations (wavelengths and oscillator strengths) are presented in Fig. 4 (curves 2–4) and Table 2. The Gaussian profiles were used for broadening in calculated spectra. The value of an FWHM was taken as 14 nm.

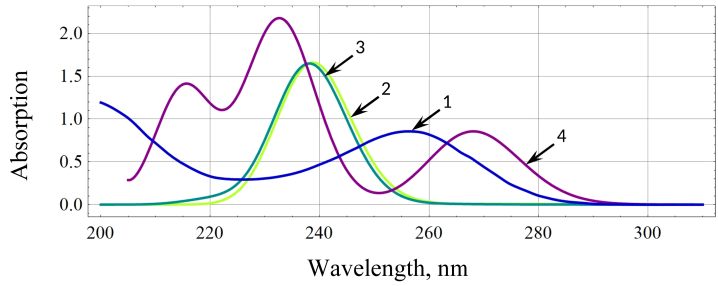

Fig. 4. Experimental (1) and calculated at the TDDFT/CAM-B3LYP/cc-pVTZ (2), TDDFT/CAM-B3LYP/cc-pVTZ+SMD (ethanol) (3), and CASSCF(4,5)/XMCQDPT2 (4) levels of theory spectra of the title compound.

Table 2. Wavelengths (λ) and oscillator strengths (f) of electronic transitions calculated at the CAM-B3LYP/cc-pVTZ, CAM-B3LYP/cc-pVTZ + SMD (ethanol) and CASSCF(4,5)/XMCQDPT2 level of theory.

	CAM-B3LYP/cc-pVTZ		CAM-B3LYP/cc-pVTZ + SMD		CASSCF(4,5)/XMCQDPT2	
Transition	λ, nm	f	λ, nm	f	λ, nm	f
$S_1 \leftarrow S_0$	277	0.001	263	0.001	268	0.001
$S_2 \leftarrow S_0$	254	0.001	238	0.281	233	0.003
$S_3 \leftarrow S_0$	242	0.016	233	0.007	215	0.002
$S_4 \leftarrow S_0$	240	0.059	226	0.001	188	0.336
$S_5 \leftarrow S_0$	238	0.153	221	0.012	118	0.000

The intensities of calculated bands were normalized. Note that the title compound comprises different functional groups (for example, phenyl, piperazine and triazole), which can exhibit ICT. This aspect was taken into account on the step of choosing the methods of calculation and interpretation of the electronic absorption spectra. Although the functional CAM-B3LYP provides the possibility of accounting of ICT in molecules,[39] it is not always successful in predicting of the UV/Vis spectra. The TDDFT calculations in the terms of the CAM-B3LYP functional of the UV/Vis spectra of the title compound predict a high value of wavelengths for $S_1 \leftarrow S_0$ (277 nm) and $S_2 \leftarrow S_0$ (254 nm) transitions with low intensity (see Table 2). Moreover, for the gas phase, the main contributions to the $S_1 \leftarrow S_0$ transition were made by the following molecular orbitals (MOs): HOMO $-$ 1 $\rightarrow$ LUMO + 1 (with a weight 5.5%), HOMO $-$ 1 $\rightarrow$ LUMO + 2 (84.5%), HOMO $-$ 1 $\rightarrow$ LUMO + 3 (2.3%), HOMO $-$ 1 $\rightarrow$ LUMO + 4 (3.4%). For the $S_2 \leftarrow S_0$ transition, the main pair of MOs is HOMO $\rightarrow$ LUMO with a weight 95.5%.

The mentioned MOs are shown in Fig. 5, and these MOs are localized not on the only one functional group (chromophore), but rather are delocalized on several ones (for example, on the sulfur atom, triazole and phenyl rings). When taking into account the solvent (ethanol), a hypsochromic shift is observed (for example, for

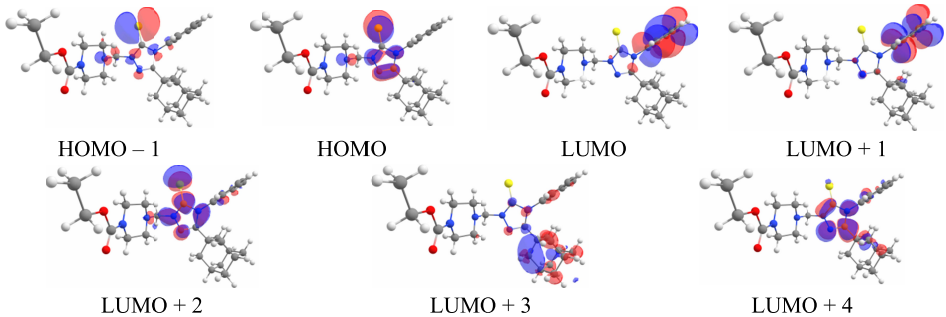

Fig. 5. Molecular orbitals contributing into $S_1 \leftarrow S_0$ and $S_2 \leftarrow S_0$ transitions, obtained at the CAM-B3LYP/cc-pVTZ level of theory.

$S_1 \leftarrow S_0$ transition, it is equal to 14 nm). It would seem that the solvent effects have to provide more correct results, which are in agreement with the experimental spectrum. However, the predicted wavelengths are still overestimated, and the intensity of the $S_2 \leftarrow S_0$ transition (oscillator strength) is increased more than 280 times. In formation of $S_1 \leftarrow S_0$ transition the HOMO $-$ 2 $\rightarrow$ LUMO + 2 with weight 2.6%, HOMO $-$ 1 $\rightarrow$ LUMO + 1 (9.2%) and HOMO $-$ 1 $\rightarrow$ LUMO + 2 (83.4%) MOs took part, and the combination of MOs HOMO $\rightarrow$ LUMO (3.5%), HOMO $\rightarrow$ LUMO + 1 (8.3%) and HOMO $\rightarrow$ LUMO + 2 (81.9%) was obtained for $S_2 \leftarrow S_0$ transition.

We assume that the incorrect prediction of UV/Vis absorption spectrum of the title compound by TDDFT method, even with the CAM-correction, is associated with ICT, the character of which is partially reflected through MOs involved in the transitions (Fig. 5).

Let us consider in detail the results of calculations of the UV/Vis spectrum obtained at the CASSCF(4,5)/XMCQDPT2 level of theory. The long-wavelength absorption band was obtained at 268 nm ($S_1 \leftarrow S_0$), and the shortwave band corresponding to the $S_2 \leftarrow S_0$ transition was predicted at 233 nm. The intensities of the calculated transitions turned out to be relatively small (see Table 2).

Some words about the choice of the active space should be said. There are several chromophores in the title molecule (= S, phenyl ring and triazole ring), which, as we expect, may be responsible for optical transitions. We are also interested in the $S_1 \leftarrow S_0$ and $S_2 \leftarrow S_0$ transitions, which were assumedly registered in the solution. Thus, we decide that those molecular orbitals, which are localized on the mentioned chromophores and which contribute to the $S_1 \leftarrow S_0$ and $S_2 \leftarrow S_0$ transitions, should be included in the active space. A quantitative description of the active space is related to the occupation of the orbitals: the orbitals, whose occupation is very close to 2.00 or 0.00, should be ignored, as well as the electrons on these orbitals, since they will not practically participate in optical transitions. So, as a result of our calculation at the CASSCF level of theory, for the selected active space of 4 electrons in 5 orbitals, the occupations of molecular orbitals were: 1.97 (1st MO), 1.20 (2nd MO),

0.41 (3rd MO), 0.40 (4th MO), 0.02 (5th MO). Also, these five MOs were localized on the three already mentioned chromophores. Thus, the selected active space is fully consistent with the qualitative and quantitative description of the transitions under consideration.

At the first stage of calculations, MOs in the active space were common for all states (due to the state-averaging procedure). However, after taking into account the dynamic component of the electron correlation energy, the MOs of the active space for each of the state became individual. Figures 6–8 show the natural MOs for the ground, first and second excited singlet states, the numbers indicate the occupancy of the MOs for each state.

Although it is not possible to select certain MOs corresponding to, for example HOMO or LUMO, within the multi-reference approach, population values, which significantly differ from 0 and 2, indicate orbitals that give the maximum contribution to electron transfer. Let us pay attention to the shape and localization of the natural MOs dominating the transitions. For the $S_1 \leftarrow S_0$ transition, the main

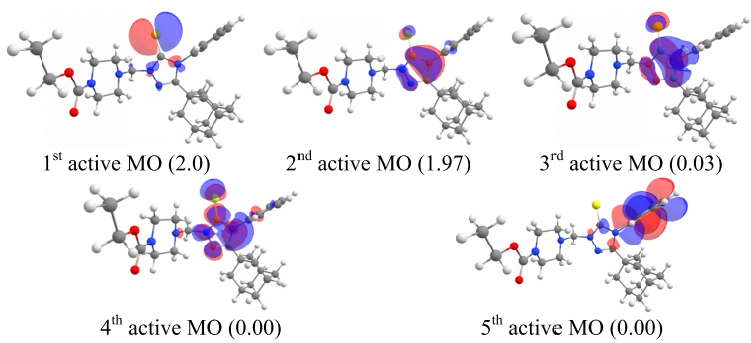

Fig. 6. Natural molecular orbitals of the active space and their respective occupations obtained for the ground state S_0 at the CASSCF(4,5)/XMCQDPT2 level of theory.

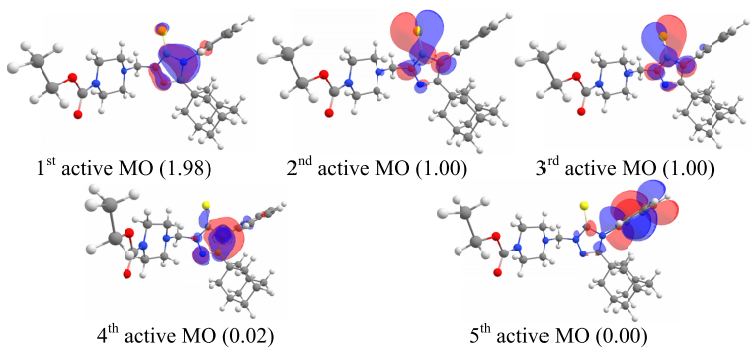

Fig. 7. Natural molecular orbitals of the active space and their respective occupations obtained for the first singlet excited state S_1 at the CASSCF(4,5)/XMCQDPT2 level of theory.

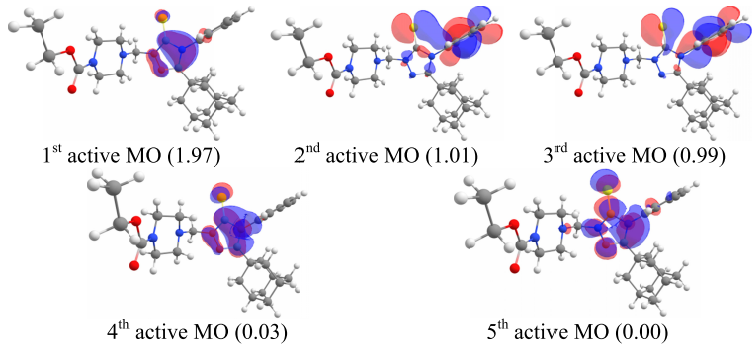

Fig. 8. Natural molecular orbitals of the active space and their respective occupations obtained for the second singlet excited state S_2 at the CASSCF(4,5)/XMCQDPT2 level of theory.

contribution is made by 2nd and 3rd active orbitals of the first excited state (Fig. 7). The shape of the molecular orbitals and the contribution of the dominant atomic orbitals indicate the $n \rightarrow \pi^*$ transition type. Lone pair electrons localized on the sulfur atom leads to the formation of a nonbonding MO, which is easily excited. The antibonding π^* orbital is localized on the triazole group. Due to the small spatial overlap of MOs, the intensity of such a transition is not high, which is reflected in the small value of the oscillator strength of the corresponding transition (see Table 2). The $S_2 \leftarrow S_0$ transition is also a low-intensity $n \rightarrow \pi^*$ transition type: the easily excited unshared valence electrons of the nonbonding MO transfer to the next energetically favorable vacant π^* orbital delocalized on the phenyl ring (see 2nd and 3rd MOs at Fig. 7). We will not discuss the high-lying excited singlet states and transitions to the ground state, related to them, since only the ground state (S_0) and the first two excited (S_1, S_2) singlet states participated in the SA-CASSCF procedure over five states (namely, three singlet and two triplet states).

It should be noted that the calculation in the multi-reference approximation was carried out for the gas phase, but the absorption UV/Vis spectrum of the title compound was measured in a polar ethanol solution. A well-known fact is the effect of the solvent on the $n \rightarrow \pi^*$ transition.[57] When using more polar media (in contrast to the $\pi \rightarrow \pi^*$ transition, which leads to a shift to the long-wavelength region of the spectrum) for the $n \rightarrow \pi^*$ transition, a hypsochromic shift (blue shift) of the corresponding bands in the UV/Vis spectrum is observed. This is due to the stabilization of the ground state by the polar solvent (for example, through hydrogen bonds), which leads to a decrease of the ground state energy, while the effect of the solvent on the excited state energy is insignificant. Thus, an increase in the energy difference between the ground and excited states leads to a decrease in the wavelength of the electron transition and the observed blue shift. Given the above, the spectrum obtained in the framework of the multi-reference approximation, taking into account the hypsochromic shift, is completely in agreement with the experimental spectrum.

ICT can be efficiently analyzed using atomic populations according to Mulliken and/or Löwdin. It is known that the atomic population strongly depends on the basis set,[36] however, we are not interested in the absolute values of charges localized on atoms, but in changes in charges delocalized on functional groups as a result of electronic transitions. Both methods of analyzing atomic populations showed charge transfer ($0.8e$ for Mulliken and $0.7e$ for Löwdin), occurring from the sulfur atom to the triazole ring as a result of the $S_1 \leftarrow S_0$ transition. The $S_2 \leftarrow S_0$ transition is also characterized by a charge transfer of $0.8e$ for both methods from the sulfur atom to the phenyl ring. Thus, sulfur in this molecule acts as a donor of electrons, and the triazole and phenyl rings as acceptors that accept these electrons, which is consistent with the analysis of natural molecular orbitals with maximum contribution to the electronic transitions under consideration.

4.4. *Biological activities*

The indices of biological activities of the studied compound (the probabilities of the presence of Pa or the absence of Pi activity of a certain type) determined by using the PASS Online database are listed in Table 3. If the index $Pa > 0.7$, then the compound under study will most likely demonstrate this kind of activity in the experiment; if $0.5 < Pa < 0.7$, the compound is likely to show activity in the experiment, but the probability is less; and, if $Pa < 0.5$, it is unlikely that the compound will demonstrate this activity in the experiment.[44] The probabilities of the biological activities Pa are given in Table 3 for values greater than 0.5. These data indicate that the compound most likely possesses analgesic ($Pa > 0.8$) and antiatherosclerotic activities ($Pa > 0.7$). The probabilities of adverse or toxic effects for this compound are small. It should be noted that the PASS program cannot predict whether a particular substance will become a drug, since creating drugs is a rather complicated task and depends on a number of different factors. But prediction, however, can help to determine for which type of biological activity should the compound be tested firstly and which substances are most likely to show the required types of activity.

Table 3. The largest indices of biological activities of compound under study predicted by PASS database.

Possible biological activities		
Pa	Pi	Activity
0.845	0.005	Analgesic
0.786	0.005	Analgesic, nonopioid
0.725	0.005	Atherosclerosis treatment
0.597	0.020	Antiviral (Picornavirus)
0.592	0.004	Calcium channel *N*-type blocker

5. Conclusions

The comprehensive spectral and theoretical analysis of the adamantane-triazole hybrid derivative, namely, ethyl 4-[3-(adamantan-1-yl)-4-phenyl-5-sulfanylidene-4,5-dihydro-1H-1,2,4-triazol-1-yl]methylpiperazine-1-carboxylate, has been carried out. The experimental IR and Raman spectra for the crystalline phase have been analyzed and interpreted based on quantum chemical modeling at the B3LYP/cc-pVTZ level of theory. Contributions from the adamantyl, phenyl, triazole, and piperazine groups within the molecule are identified. The UV/Vis spectra simulations at the TDDFT and MRPT levels of theory have demonstrated unsuitability of the first approximation (namely TDDFT) for description of the experimental spectrum of the title molecule. It is highly probable that this is a consequence of the ICT. The results obtained by second approximation (namely MRPT) have been in agreement with the experimental spectrum. The presence of the ICT was verified by Mulliken and Löwdin atomic population analysis, which has shown the charge transfer occurring from sulfur atom (donor) to triazole and phenyl rings (acceptors). Also, the indices of the biological activities were calculated based on the molecular structure and showed that the title compound is likely to possess analgesic and antiatherosclerotic activities. The results obtained could be useful for medicinal chemistry and for analytical purposes.

Acknowledgment

This work has been supported by the Belarusian Republican Foundation for Fundamental Research (Nr. F18MS-046).

References

1. Lamoureux G, Artavia G, Use of the adamantane structure in medicinal chemistry, *Curr Med Chem* **17**:2967–2978, 2010.
2. Liu J, Obando D, Liao V, Lifa T, Codd R, The many faces of the adamantyl group in drug design, *Eur J Med Chem* **46**:1949–1963, 2011.
3. Wanka L, Iqbal K, Schreiner PR, The lipophilic bullet hits the targets: Medicinal chemistry of adamantane derivatives, *Chem Rev* **113**:3516–3604, 2013.
4. Davies WL, Grunnert RR, Haff RF, McGahen JW, Neumeyer EM, Paulshock M, Watts JC, Wood TR, Hermann EC, Hoffmann CE, Antiviral activity of 1-adamantamine (amantadine), *Science* **144**:862–863, 1964.
5. Schwab RS, England AC Jr, Poskanzer DC, Young RR, Amantadine in the treatment of Parkinson's disease, *J Am Med Assoc* **208**:1168–1170, 1969.
6. Rosenthal KS, Sokol MS, Ingram RL, Subramanian R, Fort RC, Tromantadine: Inhibitor of early and late events in herpes simplex virus replication, *Antimicrob Agents Chemother* **22**:1031–1036, 1982.
7. Stylianakis I, Kolocouris A, Kolocouris N, Fytas G, Foscolos GB, Padalko E, Neyts J, De Clercq E, Spiro[pyrrolidine-2,2'-adamantanes]: synthesis, anti-influenza virus activity and conformational properties, *Bioorg Med Chem Lett* **13**:1699–1703, 2003.
8. Zoidis G, Fytas C, Papanastasiou I, Foscolos GB, Fytas G, Padalko E, De Clercq E, Naesens L, Neyts J, Kolocouris N, Heterocyclic rimantadine analogues with antiviral activity, *Bioorg Med Chem* **14**:3341–3348, 2006.

9. El-Emam AA, Al-Deeb OA, Al-Omar MA, Lehmann J, Synthesis, antimicrobial, and anti-HIV-1 activity of certain 5-(1-adamantyl)-2-substituted thio-1,3,4-oxadiazoles and 5-(1-adamantyl)-3-substituted aminomethyl-1,3,4-oxadiazoline-2-thiones, *Bioorg Med Chem* **12**:5107–5113, 2004.
10. Balzarini J, Orzeszko B, Mauri JK, Orzeszko A, Synthesis and anti-HIV studies of 2-adamantyl-substituted thiazolidin-4-ones, *Eur J Med Chem* **42**:993–1003, 2007.
11. Sun SY, Yue P, Chen X, Hong WK, Lotan R, The synthetic retinoid CD437 selectively induces apoptosis in human lung cancer cells while sparing normal human lung epithelial cells, *Cancer Res* **62**:2430–2436, 2002.
12. Lorenzo P, Alvarez R, Ortiz MA, Alvarez S, Piedrafita FJ, de Lera ÁR, Inhibition of IκB kinase-β and anticancer activities of novel chalcone adamantyl arotinoids, *J Med Chem* **81**:5431–5440, 2008.
13. Riganas S, Papanastasiou I, Foscolos GB, Tsotinis A, Bourguignon J-J, Serin G, Mirjolet J-F, Dimas K, Kourafalos VN, Eleutheriades A, Moutsos VI, Khan H, Georgakopoulou S, Zaniou A, Prassa M, Theodoropoulou M, Pondiki S, Vamvakides A, Synthesis, σ1, σ2-receptors binding affinity and antiproliferative action of new C1-substituted adamantanes, *Bioorg Med Chem* **20**:3323–3331, 2012.
14. Protopopova M, Hanrahan C, Nikonenko B, Samala R, Chen P, Gearhart J, Einck L, Nacy CA, Identification of a new antitubercular drug candidate, SQ109, from a combinatorial library of 1,2-ethylenediamines, *J Antimicrob Chemother* **56**:968–974, 2005.
15. El-Emam AA, Al-Tamimi A-MS, Al-Omar MA, Alrashood KA, Habib EE, Synthesis and antimicrobial activity of novel 5-(1-adamantyl)-2-aminomethyl-4-substituted-1,2,4-triazoline-3-thiones, *Eur J Med Chem* **68**:96–102, 2013.
16. Omar K, Geronikaki A, Zoumpoulakis P, Camoutsis C, Sokoviċ M, Ćirić A, Glamoćlija J, Novel 4-thiazolidinone derivatives as potential antifungal and antibacterial drugs, *Bioorg Med Chem* **18**:426–432, 2010.
17. Al-Abdullah ES, Asiri HH, Lahsasni S, Habib EE, Ibrahim TM, El-Emam AA, Synthesis, antimicrobial, and anti-inflammatory activity, of novel S-substituted and N-substituted 5-(1-adamantyl)-1,2,4-triazole-3-thiols, *Drug Des Dev Ther* **8**:505–518, 2014.
18. Dong Y, Wittlin S, Sriraghavan K, Chollet J, Charman SA, Charman WN, Scheurer C, Urwyler H, Tomas JS, Snyder C, Creek DJ, Morizzi J, Koltun M, Matile H, Wang X, Padmanilayam M, Tang Y, Dorn A, Brun R, Vennerstrom JL, The structure-activity relationship of the antimalarial ozonide arterolane (OZ277), *J Med Chem* **53**:481–491, 2010.
19. Kouatly O, Geronikaki A, Kamoutsis C, Hadjipavlou-Litina D, Eleftheriou P, Adamantane derivatives of thiazolyl-N-substituted amide, as possible non-steroidal anti-inflammatory agents, *Eur J Med Chem* **44**:1198–1204, 2009.
20. Al-Deeb OA, Al-Omar MA, El-Brollosy NR, Habib EE, Ibrahim TM, El-Emam AA, Synthesis, antimicrobial, and anti-inflammatory activities of novel 2-[3-(1-adamantyl)-4-substituted-5-thioxo-1,2,4-triazolin-1-yl]acetic acids, 2-[3-(1-adamantyl)-4-substituted-5-thioxo-1,2,4-triazolin-1-yl]propionic acids and related derivatives, *Arzneim-Forsch/Drug Res* **56**:40–47, 2006.
21. Augeri DJ, Robl JA, Betebenner DA, Magnin DR, Khanna A, Robertson JG, Wang A, Simpkins LM, Taunk P, Huang Q, Han S, Abboa-Offei B, Cap M, Xin L, Tao L, Tozzo E, Welzel GE, Egan DM, Marcinkeviciene J, Chang SY, Biller SA, Kirby MS, Parker RA, Hamann LG, Discovery and preclinical profile of saxagliptin (BMS-477118): A highly potent, long-acting, orally active dipeptidyl peptidase IV inhibitor for the treatment of type 2 diabetes, *J Med Chem* **48**:5025–5037, 2005.
22. Pasqualotto AC, Thiele KO, Goldani LZ, Novel triazole antifungal drugs: Focus on isavuconazole, ravuconazole and albaconazole, *Curr Opin Investig Drugs* **11**:165–174, 2010.

23. Navidpour L, Shafaroodi H, Abdi K, Amini M, Ghahremani MH, Dehpour AR, Shafiee A, Design, synthesis, and biological evaluation of substituted 3-alkylthio-4,5-diaryl-4*H*-1,2,4-triazoles as selective COX-2 inhibitors, *Bioorg Med Chem* **14**:2507–2517, 2006.
24. Hou Y, Sun J, Pang Z, Lv P, Li D, Yan L, Zhang H, Zheng EX, Zhao J, Zhu H, Synthesis and antitumor activity of 1,2,4-triazoles having 1,4-benzodioxan fragment as a novel class of potent methionine aminopeptidase type II inhibitors, *Bioorg Med Chem* **19**:5948–5954, 2011.
25. Shundalau MB, Al-Abdullah ES, Shabunya-Klyachkovskaya EV, Hlinisty AV, Al-Deeb OA, El-Emam AA, Gaponenko SV, Raman, infrared and DFT studies of N'-(adamantan-2-ylidene)benzohydrazide, a potential antibacterial agent, *J Mol Struct* **1115**:258–266, 2016.
26. Andrianov AM, Kashyn IA, Andrianov VM, Shundalau MB, Hlinisty AV, Gaponenko SV, Shabunya-Klyachkovskaya EV, Matsukovich AS, Al-Tamimi A-MS, El-Emam AA, Structure of N'-(adamantan-2-ylidene)benzohydrazide, a potential antibacterial agent, in solution: Molecular dynamics simulations, quantum chemical calculations and Ultraviolet–visible spectroscopy studies, *J Chem Sci* **128**:1933–1942, 2016.
27. Mindarava YL, Shundalau MB, Al-Wahaibi LH, El-Emam AA, Matsukovich AS, Gaponenko SV, Spectral analysis of 3-(adamantan-1-yl)-4-ethyl-1-[(4-phenylpiperazin-1-yl)methyl]-1H-1,2,4-triazole-5(4H)-thione, *J Appl Spectrosc* **85**:203–215, 2018.
28. Shundalau MB, Mindarava YL, Matsukovich AS, Gaponenko SV, El-Emam AA, Alkahtani HM, Structural, vibrational and UV/Vis studies of adamantane-containing triazole thiones by spectral, DFT and multi-reference *ab initio* methods, *Z Phys Chem* **233**: 2019.
29. Al-Abdullah ES, Asiri HH, El-Emam AA, Ng SW, Ethyl 4-[3-(adamantan-1-yl)-4-phenyl-5-sulfanylidene-4,5-dihydro-1H-1,2,4-triazol-1-yl]methylpiperazine-1-carboxylate, *Acta Cryst* **E68**:o531, 2012.
30. Schmidt MW, Baldridge KK, Boatz JA, Elbert ST, Gordon MS, Jensen JH, Koseki S, Matsunaga N, Nguyen KA, Su SJ, Windus TL, Dupuis M, Montgomery JA Jr, General atomic and molecular electronic structure system, *J Comp Chem* **14**:1347–1363, 1993.
31. http://www.msg.ameslab.gov/GAMESS/GAMESS.html (2019).
32. Dunning TH Jr, Gaussian basis sets for use in correlated molecular calculations. I. The atoms boron through neon and hydrogen, *J Chem Phys* **90**:1007–1023, 1989.
33. Becke AD, Density-functional thermochemistry. III. The role of exact exchange, *J Chem Phys* **98**:5648–5652, 1993.
34. Lee C, Yang W, Parr RG, Development of the Colle-Salvetti correlation-energy formula into a functional of the electron density, *Phys Rev B* **37**:785–789, 1988.
35. Stephens PJ, Devlin FJ, Chabalowski CF, Frisch MJ, Ab initio calculation of vibrational absorption and circular dichroism spectra using density functional force fields, *J Phys Chem* **98**:11623–11627, 1994.
36. Jensen F, *Introduction to Computational Chemistry*, 2nd edn. (John Wiley, Chichester, 2007).
37. Runge E, Gross EKU, Density-functional theory for time-dependent systems, *Phys Rev Lett* **52**:997–1000, 1984.
38. Burke K, Werschnik J, Gross EKU, Time-dependent density functional theory: Past, present, and future, *J Chem Phys* **123**:062206, 2005.
39. Yanai T, Tew DP, Handy NC, A new hybrid exchange–correlation functional using the Coulomb-attenuating method (CAM-B3LYP), *Chem Phys Lett* **393**:51–57, 2004.
40. Marenich AV, Cramer CJ, Truhlar DG, Universal solvation model based on solute electron density and on a continuum model of the solvent defined by the bulk dielectric constant and atomic surface tensions, *J Phys Chem B* **113**:6378–6396, 2009.

41. Granovsky AA, Extended multi-configuration quasi-degenerate perturbation theory: The new approach to multi-state multi-reference perturbation theory, *J Chem Phys* **134**:214113, 2011.
42. Granovsky AA, Firefly version 8, http://classic.chem.msu.su/gran/firefly/index.html (2019).
43. Druzhilovskiy DS, Rudik AV, Filimonov DA, Gloriozova TA, Lagunin AA, Dmitriev AV, Pogodin PV, Dubovskaya VI, Ivanov SM, Tarasova OA, Bezhentsev VM, Murtazalieva KA, Semin MI, Maiorov IS, Gaur AS, Sastry GN, Poroikov VV, Computational platform Way2Drug: From the prediction of biological activity to drug repurposing, *Russ Chem Bull Int Ed* **66**:1832–1841, 2017.
44. Lagunin A, Stepanchikova A, Filimonov D, Poroikov V, PASS: Prediction of activity spectra for biologically active substances, *Bioinformatics* **16**:747–748, 2000.
45. PASS Online, http://way2drug.com/passonline/index.php (2019).
46. Kubinyi H, Chemical similarity and biological activities, *J Braz Chem Soc* **137**:17–726, 2002.
47. Hargittai I, Hedberg K, *In Molecular Structures and Vibrations*, Cyvin SJ (ed.), Elsevier, New York, 1972.
48. Larsen NW, Microwave spectra of the six mono-13C-substituted phenols and of some monodeuterated species of phenol. Complete substitution structure and absolute dipole moment, *J Mol Struct* **51**:175–190, 1979.
49. Bagrij EI, *Adamantanes*, Nauka, Moscow, 1989.
50. Bistričić L, Baranović G, Mlinarić-Majerski K, A vibrational assignment of adamantane and some of its isotopomers. Empirical versus scaled semiempirical force field, *Spectrochim Acta A* **51**:1643–1664, 1995.
51. Silverstein RM, Webster FX, Kiemle DJ, *Spectrometric Identification of Organic Compounds*, 7th edn., John Wiley, New York, 2005.
52. Hendra PJ, Powell DB, The infra-red and Raman spectra of piperazine, *Spectrochim Acta* **18**:299–306, 1962.
53. Gunasekaran S, Anita B, Spectral investigation and normal coordinate analysis of piperazine, *Indian J Pure Appl Phys* **46**:833–838, 2008.
54. Alver Ö, Parlak C, Şenyel M, FT-IR and NMR investigation of 1-phenylpiperazine: A combined experimental and theoretical study, *Spectrochim Acta A* **67**:793–801, 2007.
55. Kudchadker SA, Rao CNR, Infrared spectra & normal vibrations of isomeric triazoles, *Indian J Chem* **11**:140–142, 1973.
56. Billes F, Endrédi H, Keresztury G, Vibrational spectroscopy of triazoles and tetrazole, *J Mol Struct (Theochem)* **530**:183–200, 2000.
57. Reichardt Ch, Welton T, *Solvents and Solvent Effects in Organic Chemistry*, 4th edn. (John Wiley & Sons, Weinheim, 2011).